Synthesis of Two-Dimensional Iron Boride on Au(111)

Xiaoshuang Li(李晓霜)[1,2†], Shaozheng Yan(闫邵政)[3†], Chen Ma(马晨)[1,2], Peng Cheng(程鹏)[1,2], Baojie Feng(冯宝杰)[1,2], Zhenpeng Hu(胡振芃)[3*], Lan Chen(陈岚)[1,2*]

[1] *Institute of Physics, Chinese Academy of Sciences, Beijing 100190, China*

[2] *School of Physical Sciences, University of Chinese Academy of Sciences, Beijing 100049, China*

[3] *School of Physics, Frontiers Science Center for New Organic Matter, Academy for Advanced Interdisciplinary Studies, Nankai University, Tianjin 300071, China*

[†]These authors contributed equally.

[*]Corresponding authors. Email: lchen@iphy.ac.cn; zphu@nankai.edu.cn

Keywords: MBene, two-dimensional iron boride, molecular beam epitaxy, scanning tunneling microscopy

PACS: 68.37.Ef, 68.65.-k, 68.55.-a, 73.20.At

Abstract

Two-dimensional (2D) transition metal borides have attracted extensive attention due to their unique electronic, magnetic, and catalytic properties. In particular, 2D Fe–B systems, which are predicted as ideal 2D magnetic arrays, have never been realized successfully. Here, we report the first synthesis of 2D Fe–B monolayer on Au(111) via molecular beam epitaxy. Scanning tunneling microscopy measurements reveal the regular order and lattice periodicity of the Fe–B monolayer. First-principles calculations reproduce the key topographic and spectroscopic features, validating the proposed structural model and indicating a dominant contribution of Fe 3*d* states in the electronical bands. Further experiments reveal the 2D Fe–B monolayer can service as template for the regular physical adsorption of individual Fe adatoms. This work also establishes a bottom-up strategy for synthesizing family of 2D MBenes.

1. Introduction

The successful synthesis of crystalline ternary borides (MAB phases) has spurred growing interest in two-dimensional (2D) transition-metal borides (MBenes).[1,2] Owing to their excellent electrical conductivity, high mechanical strength, and abundant surface active sites, MBenes have emerged as promising materials for energy storage,[3,4] gas sensing,[5,6] and electrocatalysis.[7,8] Analogous to MXenes, which are typically derived by etching the A layers of MAX phases ($M_{n+1}AX_n$, M = transition metal, A = main-group element, and X = C/N),[9] MBenes can be obtained through the selective etching of layered MAB phases.[10,11] Although various synthesis routes for MBenes have been developed, inherent limitations persist.[12,13] Specifically, wet etching often involves safety concerns and may introduce structural defects,[14-17] whereas solid-state strategies are generally time-consuming and prone to yielding mixed-phase products.[18,19] Moreover, top-down approaches rely heavily on the availability of high-quality MAB precursors.[20] Meanwhile, bottom-up methods, such as chemical reduction and high-pressure vapor deposition,[12] are scarce and lack precise control over atomic thickness. Recent work has demonstrated that 2D carbon nitrides can be epitaxially grown on Cu(111) through systematic tuning of the growth parameters,[21] highlighting the potential of bottom-up epitaxial approaches for synthesizing low-dimensional binary materials, including binary MBenes.

To date, several binary MBene systems, such as MoB, CrB, and TiB, have been successfully synthesized.[14,15,17,19,22-24] However, truly 2D Fe–B systems with monolayer thickness remain largely unexplored. Nevertheless, theoretical studies have predicted a variety of 2D Fe–B structures with intriguing properties. For instance, Fe atoms embedded in β_{12}-borophene and χ_3-borophene can form 2D magnetically ordered arrays.[25] Beyond potential 2D magnetism, monolayer FeB_2 has been predicted to be a graphene-like Dirac material.[26,27] Concurrently, monolayer FeB_6 exhibits excellent structural stability,[28-30] comprising a metallic α phase and indirect-bandgap β and γ phases with strong visible-light absorption.[31,32] These theoretical predictions underscore the need for experimental realization of 2D Fe–B systems.

Here we report the epitaxial synthesis of a large-scale 2D Fe–B phase on Au(111) by molecular beam epitaxy (MBE). Scanning tunnelling microscopy (STM) measurements reveal a regular lattice arrangement in the Fe–B monolayer. First-principles calculations yield a structural model that reproduces the key topographic features observed experimentally. The calculated projected density of states (PDOS) captures the overall spectral profile. Orbital-resolved analysis further shows that the spectroscopic features around the Fermi level (E_F) primarily originate from Fe 3*d* states. We also reveal the 2D Fe–B monolayer can act as a template for the individual Fe atoms adsorption to form regular array. Beyond expanding the MBene family, this work establishes a bottom-up strategy for the synthesis of truly 2D MBenes.

2. Methods

Experiments. The experiments were performed in a home-built ultrahigh-vacuum MBE/STM system, with base pressures of approximately 5.3×10^{-11} and 1.9×10^{-10} Torr in the STM and MBE chambers, respectively. The Au(111) and Ag(111) substrates were cleaned by repeated cycles of Ar^+ ion sputtering followed by annealing at 620 and 600 K, respectively. Fe (99.99%) and B (99.9999%) were then co-deposited onto the substrates using a custom-built evaporator and a commercial electron-beam evaporator, respectively. During co-deposition, the substrates were maintained at 500 K, while the pressure in the MBE chamber was kept below 5.1×10^{-10} Torr. After growth, the samples were transferred to the STM chamber without breaking vacuum. The STM and scanning tunneling spectroscopy (STS) measurements were performed at 5 K using a nonmagnetic Pt/Ir tip. All STS data were acquired using a lock-in amplifier with a modulation voltage of 20 mV at a frequency of 667 Hz. The STM data were processed using the WSxM software.[33]

Calculations. First-principles calculations were performed within the framework of density functional theory (DFT) using the Vienna Ab initio Simulation Package (VASP).[34] The interaction between valence electrons and ionic cores was described by the projector-augmented wave (PAW) method,[35] while the exchange–correlation energy was treated within the generalized gradient approximation (GGA) using the

Perdew–Burke–Ernzerhof (PBE) functional.[36] The Kohn–Sham wavefunctions were expanded in a plane-wave basis set with a kinetic-energy cutoff of 520 eV. Brillouin-zone integrations were carried out using Monkhorst–Pack k-point meshes,[37] with the sampling density chosen to ensure a reciprocal-space spacing smaller than $2\pi \times 0.02$ $Å^{-1}$ along the periodic directions. The electronic self-consistent-field iterations were converged to within 10^{-5} eV in total energy. Atomic structures were optimized using a conjugate-gradient scheme until the residual Hellmann–Feynman force on each atom was less than 0.01 eV/Å. During structural optimization, the bottom two Au layers were fixed. The topmost Au layer and the Fe–B overlayer were fully relaxed. A vacuum region of at least 20 Å was introduced along the surface-normal (z) direction to avoids the interactions between periodic images.

3. Results and Discussion

The Ag(111) surface was the first metal substrate on which borophene was experimentally realized,[38,39] and we investigated the growth of a 2D Fe–B phase on Ag(111) firstly. After the growth of β_{12} borophene on a clean Ag(111) substrate, Fe atoms were deposited onto the β_{12}-borophene/Ag(111) surface at room temperature. Only Fe clusters and adatoms were observed on the borophene surface, as shown in Fig. 1(a). The apparent height of an individual Fe adatom relative to the β_{12}-borophene surface was approximately 98 pm [Fig. 1(b)], indicating the Fe atoms adsorb on the β_{12}-borophene directly.

To enhance atomic diffusion and surface reactivity, Fe and B were subsequently co-deposited onto the Ag(111) substrate maintained at 500 K. A relatively flat 2D structure with arbitrary bright and dark morphology was obtained, as shown in Fig. 1(c). High-resolution differential STM image [Fig. 1(d)] reveal that the dark parts exhibit regular lattice corresponding to β_{12} borophene domains, whereas the bright parts exhibit a disordered, loosely packed feature, tentatively assigned to Fe–B clusters. The STM images suggest the phase separation phenomena, indicating the preferential formation of borophene on Ag(111), which kinetically hinders the redistribution of B species required for the formation of 2D Fe–B crystalline.

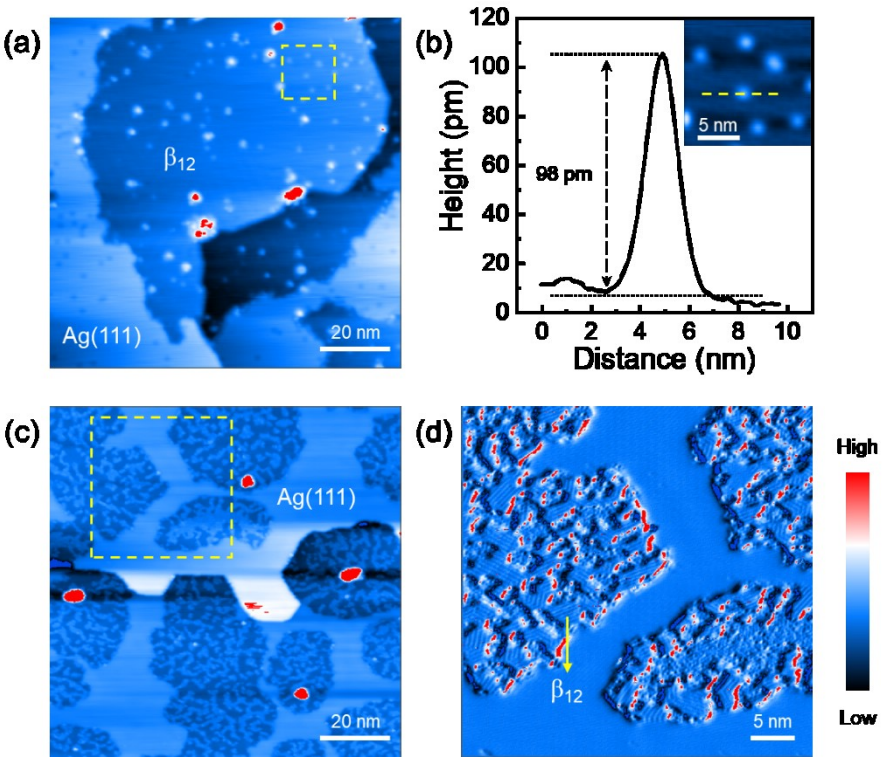


Fig. 1. Growth exploration of a 2D Fe–B phase on Ag(111). (a) Large-area STM image acquired after Fe deposition onto the Ag(111) substrate covered with β_{12}-borophene at room temperature (V_s = 1.0 V, I_s = 40 pA). (b) Line profile taken along the dashed line in the inset, revealing an apparent height of approximately 98 pm for an individual Fe atom relative to the β_{12}-borophene surface. The inset shows a high-resolution STM image of the region enclosed by the dashed square in (a). (c) Large-area STM image acquired after co-deposition of Fe and B atoms/clusters onto the Ag(111) substrate maintained at 500 K (V_s = –1.0 V, I_s = –20 pA). (d) High-resolution differential STM image of the region enclosed by the dashed square in (c), revealing the formation of β_{12} borophene sheets.

Following post-growth annealing at 590 K, the overall coverage of the islands remained unchanged, whereas their morphology evolved noticeably [Figs. S1(a) and S1(b)]. The dark parts corresponding to the β_{12} borophene transformed into the χ_3 phase with enlarged domains [Figs. S1(c) and S1(d)], consistent with the thermally driven borophene phase transition previously reported on Ag(111).[38] Meanwhile, the bright parts underwent limited coalescence upon annealing, but remained disordered.

To examine the substrate dependence of 2D Fe–B phase growth, we applied the same growth procedure and co-deposition parameters used for Ag(111) to Au(111). A large-area, ordered 2D Fe–B phase was successfully synthesized on Au(111), as shown in Figs. 2(a) and 2(b). The contrasting growth behaviors on Ag(111) and

Au(111) suggest that substrate-dependent B diffusion and redistribution influence the growth of 2D Fe–B phases. On Ag(111), the preferential formation of borophene provides a kinetically favored pathway for B–B bonding.[38,39] This may compete with Fe–B bond formation and hinder the redistribution of B species needed to form an ordered 2D Fe–B phase. In contrast, on Au(111), B atoms diffuse into the substrate at elevated temperatures, and segregate toward the surface to form borophene upon cooling.[40] This provides a distinct pathway for B redistribution, which may facilitate the co-assembly of Fe and B and favor the formation of ordered 2D Fe–B phases. Such substrate-mediated B redistribution, together with thermally driven structural evolution,[41] may ultimately enable the formation of the ordered 2D Fe–B phase on Au(111).

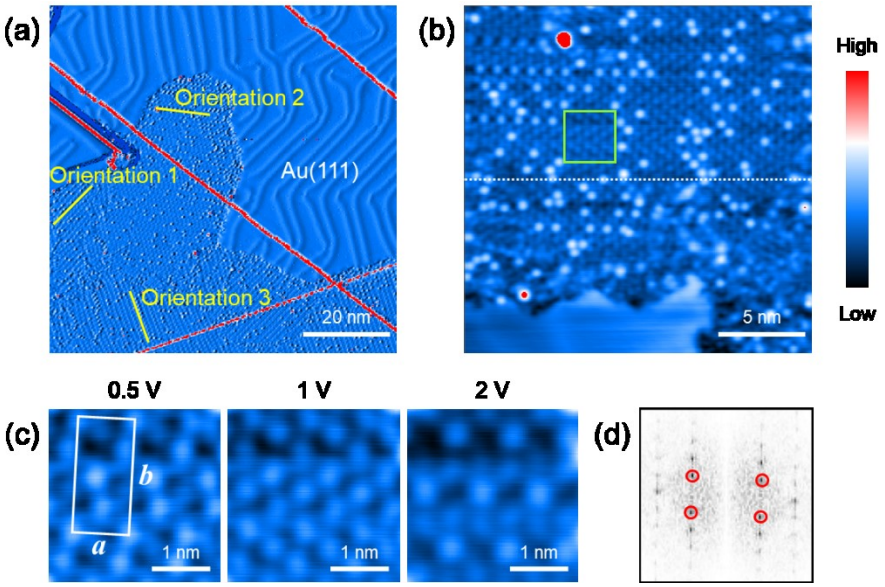


Fig. 2. Synthesis and STM characterization of a 2D Fe–B phase on Au(111). (a) Large-area differential STM image of the Fe–B phase on Au(111) (V_s = –1.0 V, I_s = –20 pA). Three domain orientations (i.e., adsorption directions) are indicated by the solid lines. (b) High-resolution STM image of a Fe–B domain (V_s = 1.0 V, I_s = 30 pA), showing a periodic array of adsorbed spots on its surface. The white dashed line marks the midline of the region. (c) A series of enlarged bias-dependent STM images of the same Fe–B region enclosed by the green square in (b). The sample biases are indicated above each panel, and the unit cell is outlined by a rectangle in the left panel. (d) FFT of the region above the white dashed line in (b). The spots enclosed by red circles correspond to the unit cell of the Fe–B phase.

Figs. 2(a) and 2(b) reveal regular lattice of Fe-B monolayer different to borophene with three equivalent rotational domains and coexisting adsorbed spots on the Fe–B monolayer. For clarity, we define the direction along which the adsorbed

spots are periodically aligned as the adsorption direction and the domain orientation. The adsorption directions are perpendicular to the <$\bar{1}$10> directions of Au(111). Figure 2(c) presents high-resolution STM images acquired on the regular Fe–B monolayer enclosed by the green square in Fig. 2(b) at different sample biases. The Fe–B monolayer exhibits a nearly rectangular unit cell with large lattice constants of a = 1.02 nm and b = 1.94 nm, with the adsorption direction parallel to the short axis (a) of the unit cell. Fast Fourier transform (FFT) of the Fe–B domain further confirms the lattice periodicity and adsorption direction [Fig. 2(d)]. The Fe–B lattice exhibits pronounced bias-dependent contrast. The protrusions in unit cell appear as alternating dumbbell-like features with opposite rotational orientations at V_s = 0.5 V, and evolve into densely packed zigzag-like chains at V_s = 1 V, and bright contrast at V_s = 2 V. This evolution of the STM contrast indicates a strong energy dependence of the local density of states (LDOS) at distinct lattice sites.[42] Furthermore, at V_s = 1 V, the ordered 2D Fe–B phase appears lower than the Au(111) terrace, whereas at V_s = 3.5 V, it appears approximately 90 pm higher than the Au(111) terrace, supporting its monolayer character [Fig. S2]. This apparent-height reversal arises from the distinct energy-dependent LDOS of the Fe–B phase and the Au(111) surface, which modify their relative contributions to the tunneling current at different sample biases.[43] In addition, the ordered 2D Fe–B phase exhibits high structural stability. Applying tip pulses of up to ~7 V at arbitrary positions within the Fe–B phase, including directly on the Fe sites, does not easily disrupt the ordered structure or induce any observable displacement of the Fe atoms.

Based on the atomic-scale STM measurements, we proposed a periodic Fe–B/Au(111) model with a chemical stoichiometry of FeB_{18}. The atomic structure is shown in Fig. 3(a). The dumbbell-like protrusions in the STM image are assigned to Fe atoms incorporated into the centers of six-membered boron rings within a 2D boron framework, while the dimmer protrusions interspersed between the "dumbbells" are associated with seven-membered boron rings. The 2D boron framework shows moderate out-of-plane corrugation, with the Fe atoms protruding 1.1 Å toward the vacuum relative to the B-plane. The DFT-optimized lattice

parameters of unit cell are a_1 = 0.98 nm and b_1 = 1.99 nm, in agreement with the experimental values. The simulated STM image reproduces the key features observed in the experimental STM image [Fig. 3(b)], suggesting the reliability of the proposed structural model.

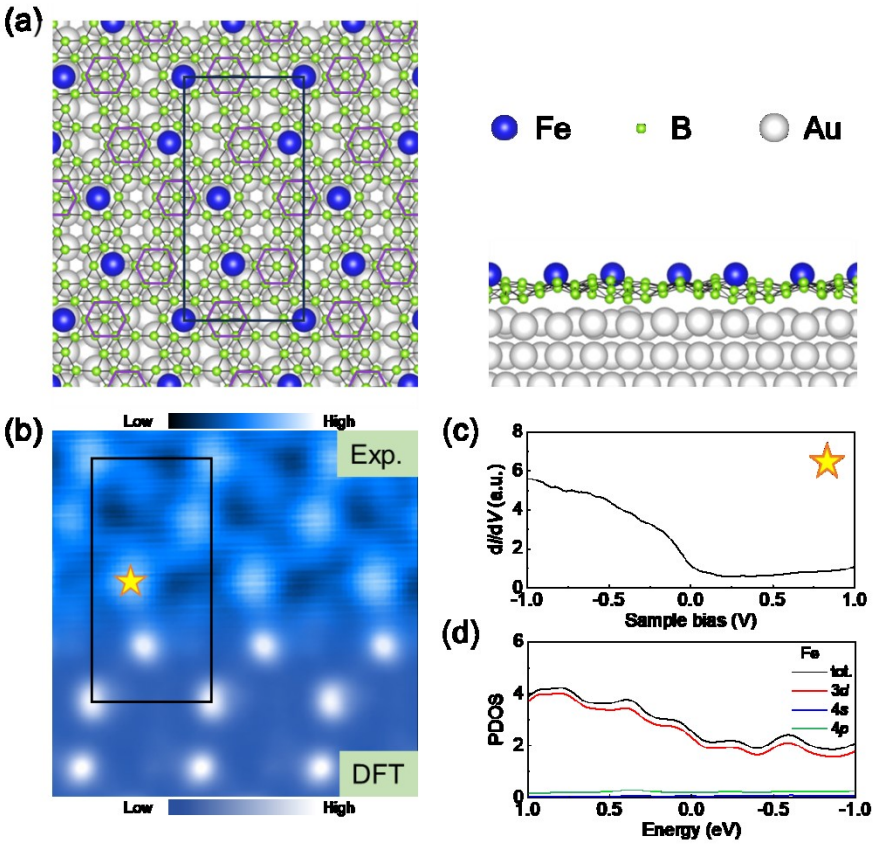


Fig. 3. Proposed structural model of the 2D Fe–B layer on Au(111). (a) Top (left) and side (right) views of the proposed structural model. Iron, boron, and gold atoms are represented by blue, green, and white spheres, respectively. The unit cell of the Fe–B layer is outlined by a black rectangle, and the seven-membered boron rings are highlighted with purple hexagons. (b) Comparison of experimental (upper) and DFT-simulated (lower) STM images. (c) dI/dV spectrum acquired at the spot marked by a star in (b). (d) Fe-PDOS, including the total PDOS and contributions from the 3d, 4s, and 4p orbitals. The calculated energy scale is rigidly shifted by +0.25 eV.

Moreover, to further elucidate the electronic structure of the Fe–B system, we performed first-principles calculations on the Fe-B monolayer. Compared with the dI/dV curve acquired at the "dumbbell" sites assigned to Fe atoms [Figs. 3(b) and 3(c)], the calculated total Fe-PDOS [the tot. PDOS curve in Fig. 3(d)] captures the overall spectral profile and pronounced asymmetry of the dI/dV curve around E_F, further validating the proposed structural model. Orbital-resolved analysis of the Fe-

PDOS further shows that the Fe 3*d* orbitals provide the dominant contribution over the displayed energy range. The d*I*/d*V* spectra acquired at the four Fe sites within the unit cell of the ordered 2D Fe–B phase exhibit similar spectral profiles [Fig. S3], particularly in the vicinity of E_F, indicating only weak site dependence of their electronic structures. Taken together, these results indicate that the experimentally observed spectroscopic features in Fig. 3(c) primarily originate from Fe 3*d* states. The Fe-protruding geometry is expected to further enhance the contribution of Fe-derived states to the tunneling signal above the Fe sites. Accordingly, the Fe-PDOS provides a reasonable description of the d*I*/d*V* spectra measured at the "dumbbell" sites.

It should be noted that an energy offset of approximately 0.25 eV exists between the calculated Fe-PDOS and the experimental d*I*/d*V* spectra. This discrepancy may arise from differences in interfacial charge transfer and energy-level alignment between the experimental interface and the idealized computational model. Finite slab thickness and local structural variations in the experimental system may also contribute to this offset. For comparison, the calculated Fe-PDOS was therefore rigidly shifted by +0.25 eV. This shift does not affect the assignment of the main spectroscopic features to Fe 3*d* states. The calculated projected band structures of the ordered 2D Fe–B phase on Au(111) are also provided in Fig. S4 to further elucidate its electronic structure, showing the predominant contribution of Fe 3*d* states near E_F.

Figure 4(a) shows a representative region of the Fe–B phase with a relatively high density of adsorbed spots. Along the adsorption direction, the spots are equidistantly aligned in a straight line with a nearest-neighbor spacing of *a*. Perpendicular to this direction, they form a uniformly spaced zigzag-like arrangement with a next-nearest-neighbor separation of *b*. These observations indicate that the adsorbed spots preferentially occupy specific periodic sites of the Fe–B lattice, consistent with the high-resolution STM images [Fig. 2(b) and Fig. S5(a)].

The adsorbed spots on the Fe–B phase were tentatively identified as Fe adatoms based on the following experimental observations. First, all spots exhibit a circular shape with nearly identical lateral dimensions, ruling out the possibility of impurity clusters. Their apparent height is approximately 95 pm above the Fe–B surface [Fig.

4(b)], consistent with that of Fe adatoms on β_{12} borophene of Ag(111) [Fig. 1(b)]. Second, individual spots can be "picked up" from the Fe–B surface by tip manipulation [Fig. 4(c)]. Specifically, the manipulation was achieved by adjusting the tunneling conditions (V_s = 50 mV, I_s = 300 pA) to approach the STM tip to the spot, followed by a relatively small voltage pulse of 2.5 V. This behavior is similar to the previously reported tip-manipulation of Fe adatoms on the Ta(100)-O surface.[44] Taken together, these results support the assignment of the adsorbed spots to Fe individual adatoms physically adsorbed on the Fe–B lattice.

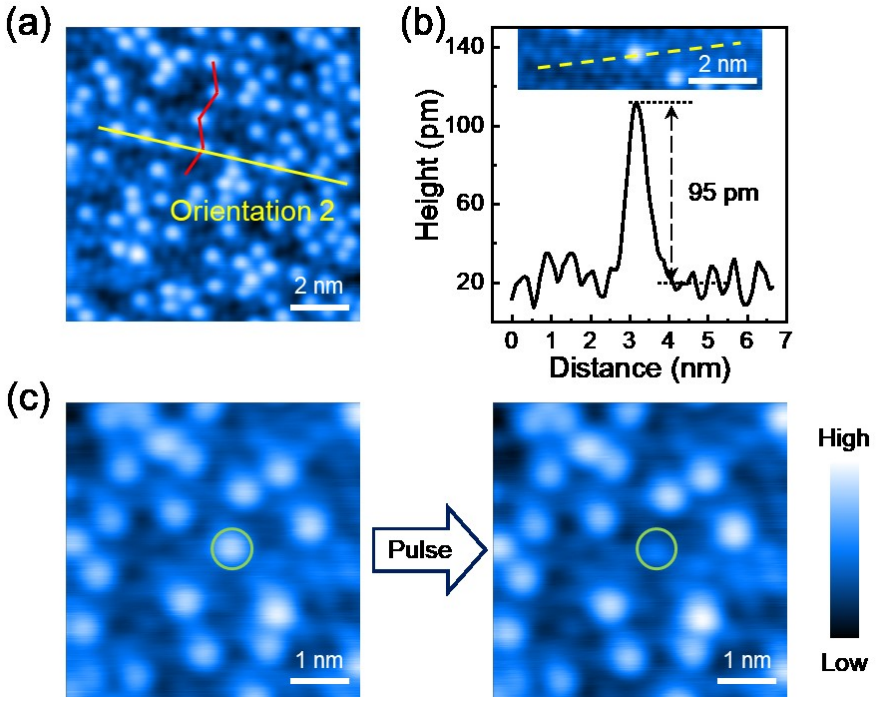


Fig. 4. Adsorbed spots and tip manipulation. (a) STM image of a Fe–B region with a relatively high density of adsorbed spots. The spots arranged along adsorption direction and the direction perpendicular to it are indicated by a yellow straight line and a red zigzag line, respectively. (b) Line profile taken along the dashed line in the inset, revealing an apparent height of approximately 95 pm for the adsorbed spot relative to the Fe–B surface. (c) STM images of the same region before (left) and after (right) tip manipulation. Green circles highlight the same site and the "picked-up" adsorbed spot.

Additional tip-manipulation experiments show that Fe adatoms initially occupying the aforementioned preferential sites can be laterally relocated by transient voltage pulses [Fig. S5(b)]. This behavior may result from the applied voltage pulses providing sufficient energy for the Fe adatoms to overcome the diffusion barrier and

migrate to metastable sites. The preferential sites are explicitly marked in the combined experimental and DFT-simulated STM image overlaid with the proposed structural model [Fig. S5(c)]. Notably, these sites correspond to the two ends of the dumbbell-like features, which are assigned to Fe sites of the ordered 2D Fe–B phase. Despite the difficulty in unambiguously identifying all metastable sites, the metastable site identified from the Fe-adatom relocation experiments shown in Fig. S5(b) is also marked in Fig. S5(c). In addition, we performed statistical analysis of a representative 2D Fe–B region with a relatively high density of Fe adatoms. The preferential-to-metastable site occupancy ratio in this region is 21:2 [Fig. S5(d)], further suggesting the energetic favorability of the preferential sites.

4. Conclusion and Outlook.

In summary, a large-scale regular 2D Fe–B monolayer was synthesized epitaxially on Au(111) by co-deposition of Fe and B atoms /clusters. The STM measurements reveal a lattice periodicity. First-principles calculations yield a structural model that reproduces the key topographic features observed experimentally. The calculated Fe-PDOS captures the overall spectral profile on the Fe atoms in unit cells. Orbital-resolved analysis further shows that the spectroscopic features around E_F primarily originate from Fe 3*d* states. Tip-manipulation experiments support the assignment of the adsorbed spots to Fe individual atoms physical-adsorbed at preferential sites of 2D Fe-B monolayer, suggesting it can act as template for the foreign atoms adsorption to form regular 2D lattice.

Moreover, applying the same growth conditions to Ag(111) yielded only phase separation of borophene domains and Fe-B disordered cluster domains, highlighting the influence of substrate-dependent interactions on 2D Fe–B phase formation, while leaving open the possibility of realizing an ordered phase through further optimization of growth parameters. Beyond expanding the MBene family, this work establishes a bottom-up strategy for the synthesis of 2D MBenes without relying on MAB precursors. The integration of magnetic atoms with boron networks may provide a promising avenue for the controlled synthesis of 2D magnetic materials in the

future.[45]

Acknowledgements.

This work was financially supported by the Ministry of Science and Technology (MOST) of China (Grant Nos. 2024YFA1409100), the National Natural Science Foundation of China (Grant Nos. 12134019, T2325028), and L.C. acknowledges the support from the CAS Project for Young Scientists in Basic Research (Grant No. YSBR-054).

References

[1] Ade M and Hillebrecht H 2015 *Inorg. Chem.* **54** 6122
[2] Kota S, Zapata-Solvas E, Ly A, Lu J, Elkassabany O, Huon A, Lee W E, Hultman L, May S J, and Barsoum M W 2016 *Sci. Rep.* **6** 26475
[3] Yuan G, Bo T, Qi X, Liu P-F, Huang Z, and Wang B-T 2019 *Appl. Surf. Sci.* **480** 448
[4] Zha X-H, Xu P, Huang Q, Du S, and Zhang R-Q 2020 *Nanoscale Adv.* **2** 347
[5] Shukla A, Sharma G, and Krishnamurty S 2023 *Appl. Surf. Sci.* **615** 156299
[6] Tan X, Na Z, Zhuo R, Wang D, Zhang Y, and Wu P 2023 *Chemosensors* **11** 371
[7] Yao M, Shi Z, Zhang P, Ong W-J, Jiang J, Ching W-Y, and Li N 2020 *ACS Appl. Nano Mater.* **3** 9870
[8] Zhu X, Zhou X, Jing Y, and Li Y 2021 *Nat. Commun.* **12** 4080
[9] VahidMohammadi A, Rosen J, and Gogotsi Y 2021 *Science* **372** eabf1581
[10] Xiong W and Dong Z 2025 *Extreme Mater.* **1** 11
[11] Zhang B, Zhou J, and Sun Z 2022 *J. Mater. Chem. A* **10** 15865
[12] Akgul E T, Altıncı O C, Umay A, Aghamohammadi P, Farghaly A A, Ma P, Chen Y, and Demir M 2024 *J. Energy Storage* **84** 110882
[13] Ramezanzadeh M, Ghamarpoor R, Dashan A, Fallah A, Soleimani S, and Ramezanzadeh B 2025 *Adv. Compos. Hybrid Mater.* **8** 269
[14] Alameda L T, Moradifar P, Metzger Z P, Alem N, and Schaak R E 2018 *J. Am. Chem. Soc.* **140** 8833
[15] Xiong W, Feng X, Xiao Y, Huang T, Li X, Huang Z, Ye S, Li Y, Ren X, Wang X, Ouyang X, Zhang Q, and Liu J 2022 *Chem. Eng. J.* **446** 137466
[16] Zhang H, Dai F-Z, Xiang H, Wang X, Zhang Z, and Zhou Y 2019 *J. Mater. Sci. Technol.* **35** 1593
[17] Zhang H, Xiang H, Dai F-z, Zhang Z, and Zhou Y 2018 *J. Mater. Sci. Technol.* **34** 2022
[18] Mou J, Li S, Zhang W, Xu W, Fan S, and Bei G 2023 *J. Adv. Ceram.* **12** 943
[19] Wang J, Ye T-N, Gong Y, Wu J, Miao N, Tada T, and Hosono H 2019 *Nat. Commun.* **10** 2284
[20] Xu T, Wang Y, Xiong Z, Wang Y, Zhou Y, and Li X 2023 *Nano-Micro Lett.* **15** 6
[21] Zhou Y, Li D, Gao Z, Zhao Q, Liu W, Gao J, Chen Y, Cheng P, Wu K, Chen L, and Feng B 2026 *Chin. Phys. Lett.* **43** 050712
[22] Bhaskar G, Gvozdetskyi V, Batuk M, Wiaderek K M, Sun Y, Wang R, Zhang C, Carnahan S L,

Wu X, Ribeiro R A, Bud'ko S L, Canfield P C, Huang W, Rossini A J, Wang C-Z, Ho K-M, Hadermann J, and Zaikina J V 2021 *J. Am. Chem. Soc.* **143** 4213
[23] Guo Z, Zhou J, and Sun Z 2017 *J. Mater. Chem. A* **5** 23530
[24] Zhou J, Palisaitis J, Halim J, Dahlqvist M, Tao Q, Persson I, Hultman L, Persson P O Å, and Rosen J 2021 *Science* **373** 801
[25] Li X, Li X, and Yang J 2019 *J. Phys. Chem. Lett.* **10** 4417
[26] Wang Z, Cheng T, and Liu Z 2022 *J. Phys. Chem. C* **126** 617
[27] Zhang H, Li Y, Hou J, Du A, and Chen Z 2016 *Nano Lett.* **16** 6124
[28] Li J, Wei Y, Fan X, Wang H, Song Y, Chen G, Liang Y, Wang V, and Kawazoe Y 2016 *J. Mater. Chem. C* **4** 9613
[29] Liu S, Huang R, Hou J, and Duan Q 2023 *Phys. Chem. Chem. Phys.* **25** 29182
[30] Wu Y, Li H, and Hou J 2021 *Comput. Mater. Sci.* **190** 110273
[31] Wang C, Zhang Y, Huang R, Wei X, Zhao X, Geng S, Xue Y, Hou J, and Duan Q 2023 *J. Mol. Model.* **29** 314
[32] Zhang H, Li Y, Hou J, Tu K, and Chen Z 2016 *J. Am. Chem. Soc.* **138** 5644
[33] Horcas I, Fernández R, Gómez-Rodríguez J M, Colchero J, Gómez-Herrero J, and Baro A M 2007 *Rev. Sci. Instrum.* **78** 013705
[34] Kresse G and Furthmüller J 1996 *Phys. Rev. B* **54** 11169
[35] Blöchl P E 1994 *Phys. Rev. B* **50** 17953
[36] Perdew J P, Burke K, and Ernzerhof M 1996 *Phys. Rev. Lett.* **77** 3865
[37] Monkhorst H J and Pack J D 1976 *Phys. Rev. B* **13** 5188
[38] Feng B, Zhang J, Zhong Q, Li W, Li S, Li H, Cheng P, Meng S, Chen L, and Wu K 2016 *Nat. Chem.* **8** 563
[39] Mannix A J, Zhou X F, Kiraly B, Wood J D, Alducin D, Myers B D, Liu X, Fisher B L, Santiago U, Guest J R, Yacaman M J, Ponce A, Oganov A R, Hersam M C, and Guisinger N P 2015 *Science* **350** 1513
[40] Kiraly B, Liu X, Wang L, Zhang Z, Mannix A J, Fisher B L, Yakobson B I, Hersam M C, and Guisinger N P 2019 *ACS Nano* **13** 3816
[41] Li S, Zhu Z, Zhang Y, Chen C, and Hu X 2025 *Chin. Phys. B* **34** 058101
[42] Klijn J, Sacharow L, Meyer C, Blügel S, Morgenstern M, and Wiesendanger R 2003 *Phys. Rev. B* **68** 205327
[43] MacLeod J M, Miwa R H, Srivastava G P, and McLean A B 2005 *Surf. Sci.* **576** 116
[44] Kamlapure A, Cornils L, Wiebe J, and Wiesendanger R 2018 *Nat. Commun.* **9** 3253
[45] Li M, Li H, and Liu S 2024 *Chin. Phys. Lett.* **41** 027501